

# Macroscopic Modeling, Calibration, and Simulation of Managed Lane-Freeway Networks, Part II: Network-scale Calibration and Case Studies

Matthew A. Wright, Roberto Horowitz, Alex A. Kurzhanskiy

## Abstract

In Part I of this paper series, several macroscopic traffic model elements for mathematically describing freeway networks equipped with managed lane facilities were proposed. These modeling techniques seek to capture at the macroscopic the complex phenomena that occur on managed lane-freeway networks, where two parallel traffic flows interact with each other both in the physical sense (how and where cars flow between the two lane groups) and the physiological sense (how driving behaviors are changed by being adjacent to a quantitatively and qualitatively different traffic flow).

The local descriptions we developed in Part I are not the only modeling complexity introduced in managed lane-freeway networks. The complex topologies mean that network-scale modeling of a freeway corridor is increased in complexity as well. The already-difficult model calibration problem for a dynamic model of a freeway becomes more complex when the freeway becomes, in effect, two interrelating flow streams. In the present paper, we present an iterative-learning-based approach to calibrating our model's physical and driver-behavioral parameters. We consider the common situation where a complex traffic model needs to be calibrated to recreate real-world baseline traffic behavior, such that counterfactuals can be generated by training purposes. Our method is used to identify traditional freeway parameters as well as the proposed parameters that describe managed lane-freeway-network-specific behaviors. We validate our model and calibration methodology with case studies of simulations of two managed lane-equipped California freeways.

**Keywords:** macroscopic first order traffic model, first order node model, multi-commodity traffic, managed lanes, HOV lanes, dynamic traffic assignment, dynamic network loading, inertia effect, friction effect, smoothing effect

## 1 Introduction

Managed lanes (Obenberger, Nov/Dec 2004), such as high-occupancy-vehicle (HOV) lanes or tolled lanes, have become a popular policy tool for transportation authorities, who seek to capture both demand management outcomes by incentivizing behaviors like carpooling (Chang et al., 2008) and to gain additional real-time control ability (Kurzhanskiy and Varaiya, 2015).

In Part I of this paper series (Wright et al., 2019), we proposed several macroscopic modeling elements for the purpose of mathematically describing a freeway equipped with a managed lane facility (a “managed lane-freeway network”). Part I discusses the road-topological considerations of modeling two parallel traffic flows, as well as mathematical descriptions for several of the complex emergent (and sometimes counteracting) phenomena that have been observed on managed lane-freeway networks, like the so-called friction (Liu et al., 2011; Jang et al., 2012; Fitzpatrick et al., 2017) and smoothing (Menendez and Daganzo, 2007; Cassidy et al., 2010; Jang and Cassidy, 2012) effects.

The present paper discusses the actual implementation of these modeling constructions. Transportation authorities considering a significant infrastructure investment like building new roads or installing managed lane facilities will make use of simulation tools during the pre-construction planning phase (Caltrans Office of Project Development Procedures, 2011). Models let transportation planners understand the characteristics of the road network, and predict outcomes of proposed modifications before their undertaking.

The use of models for the predictive study of counterfactuals is especially relevant for managed lane deployments. A major benefit of modern managed lanes to transportation authorities is how they can enable real-time, reactive control (Obenberger, Nov/Dec 2004; Kurzhanskiy and Varaiya, 2015). Managed lanes today may be instrumented with operational capabilities for real-time traffic control, such as dynamic, condition-responsive toll rates in tolled express lanes (Lou et al., 2011). Real-time control decisions can be studied via a well-tuned predictive model. As the traffic situation changes, multiple potential operational strategies can be evaluated to decide on the best course of action.

Before a traffic model can be used for forecasting or generating counterfactuals, it must be tuned to represent a base-case scenario, usually the existing traffic patterns. This process of model tuning is generally referred to as *calibration*. Calibration of traffic network models is known to be a difficult task (Treiber and Kesting, 2013, Chapter 16): vehicle traffic dynamics exhibit many complex and interacting nonlinear behaviors, and a model must realistically capture these behaviors to be useful for analysis or planning purposes. For a freeway-corridor-scale network, the data available for model calibration may consist of vehicle counts and mean speeds from vehicle detectors, origin-destination survey data, and/or descriptive information about the regular spatiotemporal extent of regular. A calibration process involves tuning a simulation model’s parameters such that it accurately reproduces typical traffic behaviors (Treiber and Kesting, 2013). The nonlinear and chaotic nature of traffic means that calibrated parameter values typically cannot be found explicitly, and must be sought after via an iterative tuning-assessment process.

In this paper, we present a calibration methodology for our recently-developed macroscopic managed lane-freeway network modeling constructions (Wright et al., 2019), that integrates them into the broader macroscopic traffic model calibration loop. Much of our focus is on identifying the split ratios, the portions of vehicles that take each of several available turns between the managed lane(s) and the general-purpose (GP) lane(s). These values are of particular importance when the behavior of the managed lane is of interest, and have major effects on the resulting analysis of managed lane usage and traffic behaviors, but are not directly measurable with traditional traffic sensors. Instead, they must be found as part of the iterative calibration process such that the macroscopic traffic patterns actually observed on the managed lane’s instrumentation are reproduced in the model. A managed lane-freeway network calibration procedure, in other words, is a *superset* of the calibration procedure for a typical freeway corridor model.

The remainder of this paper is organized as follows. Section 2 outlines the macroscopic traffic model in question, which augments the traditional kinematic-wave macroscopic traffic model with the managed-lane-specific constructions developed in Wright et al. (2019). Calibration procedures for the managed-lane-specific components, and the integration of them into a full calibration loop, is discussed in Section 3. Two case studies of macroscopic modeling of managed-lane-equipped freeways in California, one with a full-access managed lane and one with a separated managed lane with gated access, are presented in Section 4, followed by concluding points in Section 5

## 2 A Managed Lane-Freeway Network Simulation Model

In this Section, we present a macroscopic simulation algorithm for managed lane-freeway networks. This can be considered a fleshing-out of the simplified first-order macroscopic simulation method briefly outlined as context in Wright et al. (2019), with extensions made by incorporating the additional items we described in the same paper.

## 2.1 Background

“Macroscopic” traffic models are those that model traffic flows via the continuum fluid approximation (originally proposed by Lighthill and Whitham (1955a,b); Richards (1956)) as opposed to “microscopic” models that model individual vehicles (Treiber and Kesting (2013) present a relatively recent broad survey of various types of traffic models). While macroscopic models necessarily have a lower resolution than microscopic models, they make up for it in areas like shorter runtimes (making them useful for real-time operational analysis).

The present paper considers a macroscopic model for managed lane-freeway networks, based on the family of “first-order,” “kinematic wave”-type models descending from the Cell Transmission Model (Daganzo, 1994, 1995).

## 2.2 Definitions

- We have a network consisting of set of directed links  $\mathcal{L}$ , representing segments of road, and a set of nodes  $\mathcal{N}$ , which join the links.
  - A node always has at least one incoming link and one outgoing link.
  - A link may have an upstream node, a downstream node, or both.
- We have  $C$  different vehicle classes traveling in the network, with classes indexed by  $c \in \{1, \dots, C\}$ .
- Let  $t \in \{0, \dots, T\}$  denote the simulation timestep.
- In addition, while we have not covered them here, the modeler may optionally choose to define *control inputs* to the simulated system that modify system parameters or the system state. Such control inputs may represent operational traffic control schemes such as ramp metering, changeable message signs, a variable managed-lane policy, etc. In the context of this paper, we suggest including the parameterization of the friction effect and the class-switching construction of the separated-access managed lane model to be discussed in section 3.2 as control actions.

### 2.2.1 Link model definitions

Traditionally, the mathematical equations that govern the traffic flow in the links are called the “link model.”

- For each link  $l \in \mathcal{L}$ , let there be a time-varying  $C$ -dimensional state vector  $\vec{\rho}_l(t)$ , which denotes the density of the link of each of the  $C$  vehicle classes at time  $t$ .
  - Each element of this vector,  $\rho_l^c(t)$ , updates between timestep  $t$  and timestep  $t + 1$  according to (2.1).
  - Also define  $\rho_{l,0}^c$  for all  $l, c$ , the initial condition of the system.
- We define three types of links:
  - Ordinary links are those links that have both beginning and ending nodes.
  - Origin links are those links that have only an ending node. These links represent the roads that vehicles use to enter the network.
  - Destination links are those links that have only a beginning node. These links represent the roads that vehicles use to exit the network.

- For each link  $l \in \mathcal{L}$ , define the actual parametric “link model” that computes the per-class demands  $S_l^c(t) \leq \rho_l^c(t)$  (the amount of vehicles that want to exit the link at time  $t$ ) and link supply  $R_l(t)$  (the amount of vehicles that link  $l$  can accept at time  $t$ ) as functions of  $t$  and  $\vec{\rho}_l(t)$ . The particular link model equations is a modeling choice, and many authors have proposed different versions. Appendix A describes a particular example link model that will be used in the example simulations in Section 4.
- For each origin link  $l \in \mathcal{L}$ , define a  $C$ -dimensional time-varying vector,  $\vec{d}_l(t)$ , where the  $c$ -th element  $d_l^c(t)$  denotes the exogenous demand of class  $c$  into the network at link  $l$ .

### 2.2.2 Node model definitions

Analogous to the link model, the equations that govern the traffic flows through nodes (i.e., between links) are called the “node model.”

- For each node  $\nu \in \mathcal{N}$ , let  $i \in \{1, \dots, M_\nu\}$  denote the incoming links and  $j \in \{1, \dots, N_\nu\}$  denote the outgoing links.
- For each node, define  $\{\beta_{ij}^c(t) : \sum_j \beta_{ij}^c(t) = 1 \forall i, c\}$  the time-varying split ratios for each triplet  $\{i, j, c\}$ . Each split ratio may be fully defined, partially defined, or fully undefined, with the undefined split ratios typically being the ones that specify the crossflows between the managed lane(s) and the GP lane(s).
- For each node with both a managed lane link and a GP link exiting it, define a (state-dependent) split ratio solver for the managed lane-eligible vehicles. We suppose that the decision of eligible vehicles of whether or not to change between the two lane types is dependent on the local traffic conditions. Appropriate methods for determining the desired lane type as a function of the current state may include logit-style discrete choice methods (Farhi et al., 2013) or dynamic-system-based models such as the one proposed in Wright et al. (2018) and reviewed in Appendix B.
- For each node, define a “node model” that, at each time  $t$ , takes its incoming links’ demands  $S_i^c(t)$  and split ratios  $\beta_{ij}^c(t)$ , its outgoing links’ supplies  $R_j(t)$ , and other nodal parameters, and computes the flows  $f_{ij}^c(t)$ . As with the link model, the particular node model equations is a modeling choice, and much literature exists defining and analyzing different node models. In this paper, we refer to a specific node model with a relaxed first-in-first-out (FIFO) construction that has additional parameters  $\eta_{j,j}^i(t)$  (mutual restriction intervals) and  $p_i(t)$  (the incoming links’ priorities). Note also that a node model with the relaxed FIFO construction can also be used to produce the smoothing effect of managed lanes, as discussed in depth in Part I (Wright et al., 2019).

### 2.2.3 State update equation definitions

These equations define the time evolution of the states from time  $t$  to time  $t + 1$ .

- All links  $l \in \mathcal{L}$  update their states according to the equation

$$\rho_l^c(t+1) = \rho_l^c(t) + \frac{1}{L_l} (f_{l,\text{in}}^c(t) - f_{l,\text{out}}^c(t)) \quad \forall c \in \{1, \dots, C\}, \quad (2.1)$$

which is a slightly generalized form of a traditional multi-class CTM update.

- For all ordinary and destination links,

$$f_{l,\text{in}}^c(t) = \sum_{i=1}^{M_\nu} f_{il}^c(t), \quad (2.2)$$

where  $\nu$  is the beginning node of link  $l$ .

- For all origin links,

$$f_{l,\text{in}}^c(t) = d_l^c(t). \quad (2.3)$$

- For all ordinary and origin links,

$$f_{l,\text{out}}^c(t) = \sum_{j=1}^{N_\nu} f_{lj}^c(t), \quad (2.4)$$

where  $\nu$  is the ending node of link  $l$ .

- For all destination links,

$$f_{l,\text{out}}^c(t) = S_l^c(t). \quad (2.5)$$

## 2.3 Simulation algorithm

1. Initialization:

$$\begin{aligned} \rho_l^c(0) &:= \rho_{l,0}^c \\ t &:= 0, \end{aligned}$$

for all  $l \in \mathcal{L}$ ,  $c \in \{1, \dots, C\}$ .

2. Perform all control inputs that have been (optionally) specified by the modeler. For our purposes, this includes:

- (a) For each managed lane link, modify the sending function of the link model in accordance with the friction effect model. As discussed in more detail in Part I (Wright et al., 2019), for the particular link model of Appendix A, our friction effect model is to modify the sending function of a managed lane link from (A.1) to

$$S_{\text{ML}}^c(t) = \hat{v}_{\text{ML}}(t) \rho_{\text{ML}}^c(t) \min \left\{ 1, \frac{\hat{F}_{\text{ML}}(t)}{\hat{v}_{\text{ML}}(t) \sum_{c=1}^C \rho_{\text{ML}}^c(t)} \right\} \quad (2.6)$$

where the subscript ‘‘ML’’ means that the symbols refer to the parameters of the managed lane link, and where the friction-adjusted free flow speed  $\hat{v}_{\text{ML}}(t)$  and capacity  $\hat{F}_{\text{ML}}(t)$  are

$$\hat{v}_{\text{ML}}(t) = v_{\text{ML}}^f(t) - \sigma_{\text{ML}} \Delta_{\text{ML}}(t) \quad (2.7)$$

$$\hat{F}_{\text{ML}}(t) = \hat{v}_{\text{ML}}(t) \rho_{\text{ML}}^+ \quad (2.8)$$

with  $n_{\text{ML}}^+$  the high critical density (see Appendix A for the definition),  $v_{\text{ML}}^f$  is the nominal free flow speed for the managed lane link,  $\sigma_{\text{ML}} \in [0, 1]$  is the *friction coefficient* of the managed lane link (which quantifies the degree to which the friction effect exerts its influence on the vehicles in the link: Jang and Cassidy (2012) and others note that road configurations where the managed lane(s) and the GP lane(s) are more physically separated, e.g., a concrete barrier or traffic bollards instead of only a painted line, have a lower magnitude of the friction effect), and  $\Delta_{\text{ML}}(t)$  is the speed differential between the managed lane link and the GP link,

$$\Delta_{11}(t) = v_{11}^f - v_1(t-1). \quad (2.9)$$

- (b) For each managed lane link whose downstream node is a gate node in a gated-access managed lane configuration, perform class switching to ensure that vehicles realistically leave the managed lane to take a downstream offramp, as detailed in Wright et al. (2019).

3. For each link  $l \in \mathcal{L}$  and commodity  $c \in \{1, \dots, C\}$ , compute the demand,  $S_l^c(t)$  using the link’s link model.
4. For each ordinary and destination link  $l \in \mathcal{L}$ , compute the supply  $R_l(t)$  using the link model. For origin links, the supply is not used.
5. For each node  $\nu \in \mathcal{N}$  that has one or more undefined split ratios  $\beta_{ij}^c(t)$ , use the node’s split ratio solver to complete a fully-defined set of split ratios. Note that if an inertia effect model is being used, the modified split ratio solver, e.g. the one described in Appendix B, should be used where appropriate.
6. For each node  $\nu \in \mathcal{N}$ , use the node model to compute throughflows  $f_{ij}^c(t)$  for all  $i, j, c$ .
7. For every link  $l \in \mathcal{L}$ , compute the updated state  $\vec{\rho}_l(t + 1)$ :
  - If  $l$  is an ordinary link, use (2.1), (2.2), and (2.4).
  - If  $l$  is an origin link, use (2.1), (2.3), and (2.4)
  - If  $l$  is a destination link, use (2.1), (2.2), and (2.5).
8. If  $t = T$ , then stop. Otherwise, increment  $t := t + 1$  and return to step 2.

### 3 Calibrating the Managed Lane-Freeway Network Model

Typically, a traffic modeler will have some set of data collected from traffic detectors (e.g., velocity and flow readings), and will create a network topology with parameter values that allow the model to reproduce these values in simulation. Then, the parameters can be tweaked to perform prediction and analysis. For our managed lane-freeway networks, the parameters of interest are:

1. Link model parameters for each link (also called “fundamental diagram” parameters, referring to the graph drawn by the sending and receiving functions as functions of density). Calibration of a link model is typically agnostic to the node model and network topology, and there exists an abundant literature on this topic. For the purposes of the simulations in this work, we used the method of Dervisoglu et al. (2009), but any other method is appropriate.
2. Percentage of special (that is, able to access the managed lane) vehicles in the traffic flow entering the system. This parameter depends on, e.g., the time of day and location as well as on the type of managed lane. It could be roughly estimated as a ratio of the managed lane vehicle count to the total freeway vehicle count during periods of congestion at any given location (supposing of course that congestion in the GP lanes will lead the eligible vehicles to select the managed lane to avoid this congestion).
3. Inertia coefficients. These parameters affect only how traffic of different classes mixes in different links, but they have no effect on the total vehicle counts produced by the simulation.
4. Friction coefficients. How to tune these parameters is an open question. In Jang and Cassidy (2012) the dependency of a managed lane’s speed on the GP lane speed was investigated under different densities of the managed lane, and the presented data suggests that although the correlation between the two speeds exists, it is not overwhelmingly strong, below 0.4. Therefore, we suggest setting friction coefficients to values not exceeding 0.4.
5. Mutual restriction intervals for the partial FIFO constraint. It is also an open question how to estimate mutual restriction intervals from the measurement data. See the discussion in Wright et al. (2019, Section 3.2) for some guidelines. Note also that the choice of restriction intervals govern the magnitude of the smoothing effect.

## 6. Offramp split ratios.

Calibrating a traffic model, or identifying the best values of its parameters to match real-world data, is typically an involved process for all but the simplest network topologies. In particular, once we consider more than a single, unbroken stretch of freeway, the nonlinear nature and network effects of these systems means that estimating each parameter in isolation might lead to unpredictable behavior. Instead, nonlinear and/or non-convex optimization techniques such as genetic algorithms (Poole and Kotsialos, 2012), particle swarm methods (Poole and Kotsialos, 2016), and others (Ngoduy and Maher (2012); Fransson and Sandin (2012), etc.) are employed.

In the managed lane-freeway networks we have discussed, the key unknown parameters we have introduced are the offramp split ratios, item 6, which may be particularly hard to estimate as they are typically time-varying and explicitly represent driver behavior, rather than physical parameters of the road. Estimating the values of the other parameters can be done with one of many methods in the literature. The remainder of this section describes iterative methods for identification of the offramp split ratios for both the full-access and gated-access topological configurations, both of which were introduced in Part I (Wright et al., 2019).

### 3.1 Split ratios for a full-access managed lane

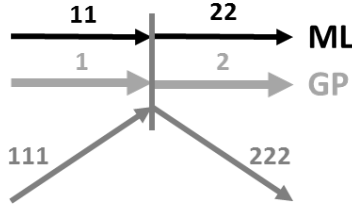


Figure 1: A node where some of the input links form travel facilities with some of the output links. ML = Managed Lane.

Consider a node, one of whose output links is an offramp, as depicted in Figure 1. We shall make the following assumptions.

1. The total flow entering the offramp,  $\hat{f}_{222}^{in}$ , at any given time is known (from measurements) and is not restricted by the offramp supply:  $\hat{f}_{222}^{in} < R_{222}$ .
2. The portions of traffic sent to the offramp from the managed lane and from the GP lane at any given time are equal:  $\beta_{1,222}^c = \beta_{11,222}^c \triangleq \beta$ ,  $c = 1, \dots, C$ .
3. None of the flow coming from the onramp (link 111), if such flow exists, is directed toward the offramp. In other words,  $\beta_{111,222}^c = 0$ ,  $c = 1, \dots, C$ .
4. The distribution of flow portions not directed to the offramp between the managed lane and the GP output links is known. This can be written as:  $\beta_{ij}^c = (1 - \beta)\delta_{ij}^c$ , where  $\delta_{ij}^c \in [0, 1]$ , as well as  $\beta_{111,j}$ ,  $i = 1, 11$ ,  $j = 2, 22$ ,  $c = 1, \dots, C$ , are known.
5. The demand  $S_i^c$ ,  $i = 1, 11, 111$ ,  $c = 1, \dots, C$ , and supply  $R_j$ ,  $j = 2, 22$ , are given.

At any given time,  $\beta$  is unknown and is to be found.

If  $\beta$  were known, the node model would compute the input-output flows, in particular,  $f_{i,222} = \sum_{c=1}^C f_{i,222}^c$ ,  $i = 1, 11$ . Define

$$\psi(\beta) = f_{1,222} + f_{11,222} - \hat{f}_{222}^{in}. \quad (3.1)$$

Our goal is to find  $\beta$  from the equation

$$\psi(\beta) = 0, \quad (3.2)$$

such that  $\beta \in \left[ \frac{\hat{f}_{222}^{in}}{S_1 + S_{11}}, 1 \right]$ , where  $S_i = \sum_{c=1}^C S_i^c$ . Obviously, if  $S_1 + S_{11} < \hat{f}_{222}^{in}$ , the solution does not exist, and the best we can do in this case to match  $\hat{f}_{222}^{in}$  is to set  $\beta = 1$ , directing all traffic from links 1 and 11 to the offramp.

Suppose now that  $S_1 + S_{11} \geq \hat{f}_{222}^{in}$ . For any given  $\hat{f}_{222}^{in}$ , we assume  $\psi(\beta)$  is a monotonically increasing function of  $\beta$  (this assumption is true for the particular node model of Wright et al. (2017)). Moreover,  $\psi\left(\frac{\hat{f}_{222}^{in}}{S_1 + S_{11}}\right) \leq 0$ , while  $\psi(1) \geq 0$ . Thus, the solution of (3.2) within the given interval exists and can be obtained using the *bisection method*.

The algorithm for finding  $\beta$  follows.

1. Initialize:

$$\begin{aligned} \underline{b}(0) &:= \frac{\hat{f}_{222}^{in}}{S_1 + S_{11}}; \\ \bar{b}(0) &:= 1; \\ k &:= 0. \end{aligned}$$

2. If  $S_1 + S_{11} \leq \hat{f}_{222}^{in}$ , then are not enough vehicles to satisfy the offramp demand. Set  $\beta = 1$  and stop.
3. Use the node model with  $\beta = \underline{b}(0)$  and evaluate  $\psi(\beta)$ . If  $\psi(\underline{b}(0)) \geq 0$ , then set  $\beta = \underline{b}(0)$  and stop.
4. Use the node model with  $\beta = \frac{\underline{b}(k) + \bar{b}(k)}{2}$  and evaluate  $\psi(\beta)$ . If  $\psi\left(\frac{\underline{b}(k) + \bar{b}(k)}{2}\right) = 0$ , then set  $\beta = \frac{\underline{b}(k) + \bar{b}(k)}{2}$  and stop.
5. If  $\psi\left(\frac{\underline{b}(k) + \bar{b}(k)}{2}\right) < 0$ , then update:

$$\begin{aligned} \underline{b}(k+1) &= \frac{\underline{b}(k) + \bar{b}(k)}{2}; \\ \bar{b}(k+1) &= \bar{b}(k). \end{aligned}$$

Else, update:

$$\begin{aligned} \underline{b}(k+1) &= \underline{b}(k); \\ \bar{b}(k+1) &= \frac{\underline{b}(k) + \bar{b}(k)}{2}. \end{aligned}$$

6. Set  $k := k + 1$  and return to step 4.

Here,  $\underline{b}(k)$  represents the lower bound of the search interval at iteration  $k$  and  $\bar{b}(k)$  the upper bound.



### 3.2 Split ratios for the separated managed lane with gated access

The configuration of a node with an offramp as one of the output links is simpler in the case of a separated managed lane, as shown in Figure 2. Here, traffic cannot directly go from the managed lane to link 222, and, thus, we have to deal only with the 2-input-2-output node. There is a caveat, however. Recall from the discussion of gated-access managed lanes in Wright et al. (2019) that in the separated managed lane case we have destination-based traffic classes, and split ratios for destination-based traffic are fixed due to being determined at an outer loop level.

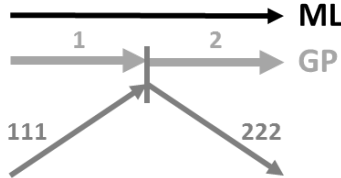


Figure 2: A node with a GP link and an onramp as inputs, and a GP link and an offramp as outputs.

We shall make the following assumptions:

1. The total flow entering the offramp,  $\hat{f}_{222}^{in}$ , at any given time is known (from measurements) and is not restricted by the offramp supply:  $\hat{f}_{222}^{in} < R_{222}$ .
2. All the flow coming from the onramp (link 111), if such flow exists, is directed toward the GP link 2. In other words,  $\beta_{111,2}^c = 1$  and  $\beta_{111,222}^c = 0$ ,  $c = 1, \dots, C$ .
3. The demand  $S_i^c$ ,  $i = 1, 111$ ,  $c = 1, \dots, C$ , and supply  $R_2$  are given.
4. We denote the set of destination-based classes as  $\mathcal{D}$ . The split ratios  $\beta_{1j}^c$  for  $c \in \mathcal{D}$  are known. Let the split ratios  $\beta_{1j}^c = \beta$  for  $c \in \{1, \dots, C\} \setminus \mathcal{D}$ , where  $\beta$  is to be determined (i.e., we assume all non-destination-based classes exit at the same rate).

The first three assumptions here reproduce assumptions 1, 3 and 5 made for the full-access managed lane case. Assumption 4 is a reminder that there is a portion of traffic flow that we cannot direct to or away from the offramp, but we have to account for it.

Similarly to the full-access managed lane case, we define the function  $\psi(\beta)$ :

$$\psi(\beta) = \sum_{c \in \overline{\mathcal{D}}} f_{1,222}^c + \sum_{c \in \mathcal{D}} f_{1,222}^c - \hat{f}_{222}^{in}, \quad (3.3)$$

where  $f_{1,222}^c$ ,  $c = 1, \dots, C$  are determined by the node model. The first term of the right-hand side of (3.3) depends on  $\beta$ . As before, we assume  $\psi(\beta)$  is a monotonically increasing function. We look for the solution of equation (3.2) on the interval  $[0, 1]$ . This solution exists iff  $\psi(0) \leq 0$  and  $\psi(1) \geq 0$ . The algorithm for finding  $\beta$  is the same as the one presented in the previous section, except that  $b(0)$  should be initialized to 0, and  $S_{11}$  is to be assumed 0.

### 3.3 An iterative full calibration process

For the purposes of the simulations presented in the following Section, we placed the iterative split ratio identification methods of Sections 3.1 and 3.2 within a larger iterative loop for the remaining parameters. The model calibration follows the flowchart shown in Figure 3.

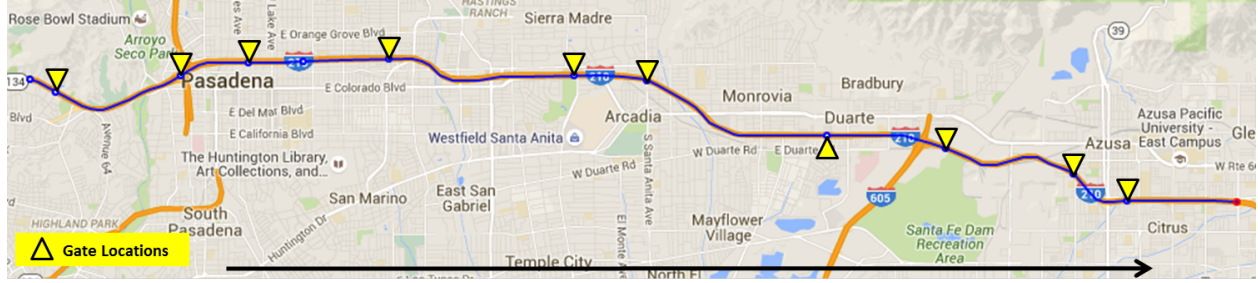


Figure 3: Calibration workflow.

1. We start by assembling the available measurement data. Fundamental diagrams are assumed to be given. Mainline and onramp demand are specified per 5-minute periods together with the special vehicle portion parameter indicating the fraction of the input demand that is able to access the managed lane. Initially, we do not know offramp split ratios as they cannot be measured directly. Instead, we use some arbitrary values to represent them and call these values “initially guessed offramp split ratios”. Instead of the offramp split ratios, we have the measured flows actually observed on the offramps, which we refer to as *offramp demand*.
2. We run our network simulation outlined in Section 2.3 for the entire simulation period. At this point, in step 5 of the simulation, the *a priori* undefined split ratios between traffic in the GP and in the managed lanes are assigned using a split ratio solver.
3. Using these newly-assigned split ratios, we run our network simulation again, only this time, instead of using the initially guessed offramp split ratios, we compute them from the given offramp demand as described in Sections 3.1 and 3.2. As a result of this step, we obtain new offramp split ratios.
4. Now we run the network simulation as we did originally, in step 2, only this time with new offramp split ratios, and record the simulation results — density, flow, speed, as well as performance measures such as vehicle miles traveled (VMT) and vehicle hours traveled (VHT).
5. Check if the resulting offramp flows match the offramp demand. If yes, proceed to step 6, otherwise, repeat steps 2-5. In our experience (i.e., the case studies in the following Section), it takes the process described in steps 2-5 no more than two iterations to converge.
6. Evaluate the simulation results:
  - correctness of bottleneck locations and activation times;
  - correctness of congestion extension at each bottleneck;
  - correctness of VMT and VHT.

If the simulation results are satisfactory, stop. Otherwise, proceed to step 7.
7. Tune/correct input data in the order shown in block 7 of Figure 3.

## 4 Simulation Results

### 4.1 Full-access managed lane case study: Interstate 680 North

We consider a 26.8-mile stretch of I-680 North freeway in Contra Costa County, California, from postmile 30 to postmile 56.8, shown in Figure 4, as a test case for the full-access managed lane configuration. This

freeway’s managed lane facilities are split into two segments whose beginning and end points are marked on the map. The first segment is a high-occupancy-tolled (HOT) lane, which allows free entry to vehicles with two or more passengers and tolled entry to single-occupancy vehicles (Metropolitan Transportation Commission, 2019), The second segment has an HOV lane is 4.5 miles long. There are 26 onramps and 24 offramps. The HOV lane is active from 5 to 9 AM and from 3 to 7 PM. The rest of the time, the HOV lane is open to all traffic, and behaves as a GP lane.

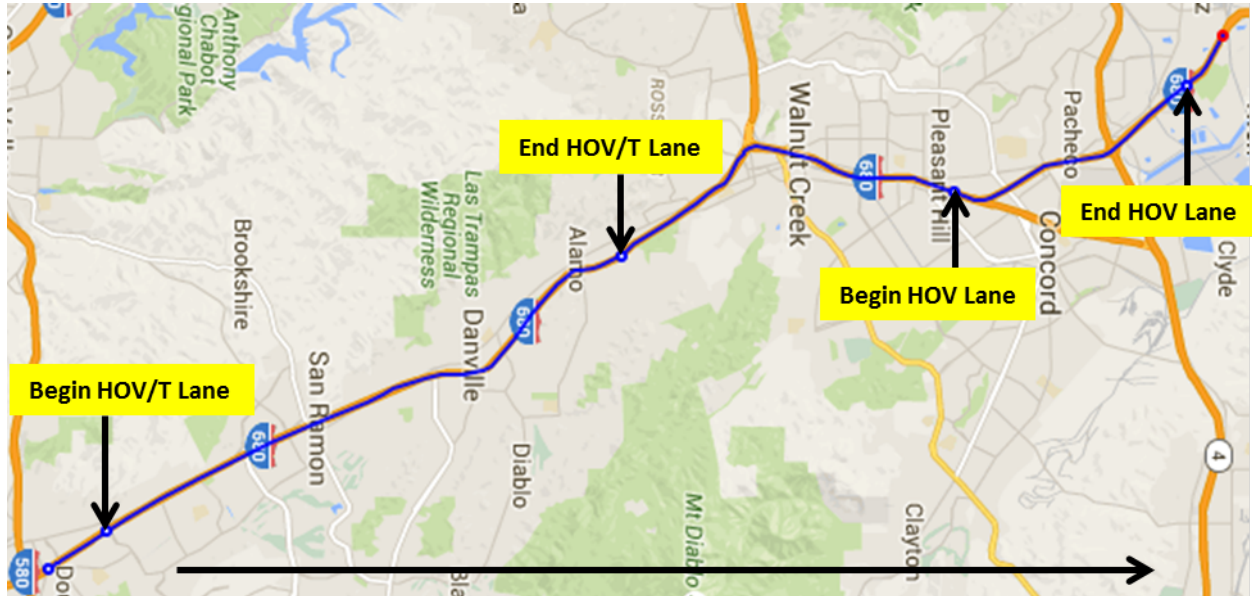


Figure 4: Map of I-680 North in Contra Costa County.

To build the model, we used data collected for the I-680 Corridor System Management Plan (CSMP) study (System Metrics Group, Inc., 2015). The bottleneck locations as well as their activation times and congestion extension were identified in that study using video monitoring and tachometer vehicle runs. On- and offramp flows were given in 5-minute increments. For the purposes of our model, we do not consider tolling dynamics, and instead assume that managed lane-eligible vehicles incur no cost to access the managed lane. We assume that the managed lane-eligible portion of the input demand is 15%. The model was calibrated to a typical weekday, as suggested in the I-680 CSMP study.

For this simulation, we used the fundamental diagram described in Appendix A, with parameters as follows:

- The capacity of the ordinary GP lane is 1,900 vehicles per hour per lane (vphl);
- The capacity of the auxiliary GP lane is 1,900 vphl;
- The capacity of the managed lane is 1,800 vphl while active and 1,900 vphl when it behaves as a GP lane;
- The free flow speed varies between 63 and 70 mph — these measurements came partially from the California Performance Measurement System (PeMS) (PeMS, 2019) and partially from tachometer vehicle runs.
- The congestion wave speed for each link was taken as 1/5 of the free flow speed.

The modeling results are presented in Figures 5, 6 and 7 showing density, flow and speed contours, respectively, in the GP and the managed lanes. In each plot, the top contour corresponds to the managed lanes,

and the bottom to the GP lanes. In all the plots traffic moves from left to right along the “Absolute Postmile” axis, while the vertical axis represents time. Bottleneck locations and congestion areas identified by the I-680 CSMP study are marked by blue boxes in GP lane contours. The managed lane does not get congested, but there is a speed drop due to the friction effect. The friction effect, when vehicles in the managed lane slow down because of the slow moving GP lane traffic, can be seen in the managed lane speed contour in Figure 7.

Figure 8 shows an example of how well the offramp flow computed by the simulation matches the target, referred to as *offramp demand*, as recorded by the detector on the offramp at Crow Canyon Road. We can see that in the beginning and in the end of the day, the computed flow falls below the target (corresponding areas are marked with red circles). This is due to the shortage of the mainline traffic in the simulation — the offramp demand cannot be satisfied.

Finally, Table 1 summarizes the performance metrics — vehicle miles traveled (VMT), vehicle hours traveled (VHT) and delay in vehicle-hours — computed by simulation versus those collected in the course of the I-680 CSMP study. Delay is computed for vehicles with speed below 45 mph.

Performance Metric	Simulation result	Collected data
GP Lane VMT	1,687,618	-
Managed Lane VMT	206,532	-
Total VMT	1,894,150	1,888,885
GP Lane VHT	27,732	-
Managed Lane VHT	3,051	-
Total VHT	30,783	31,008
GP Lane Delay (hr)	2,785	-
Managed Lane Delay (hr)	6	-
Total Delay (hr)	2,791	2,904

Table 1: Performance metrics for I-680 North.

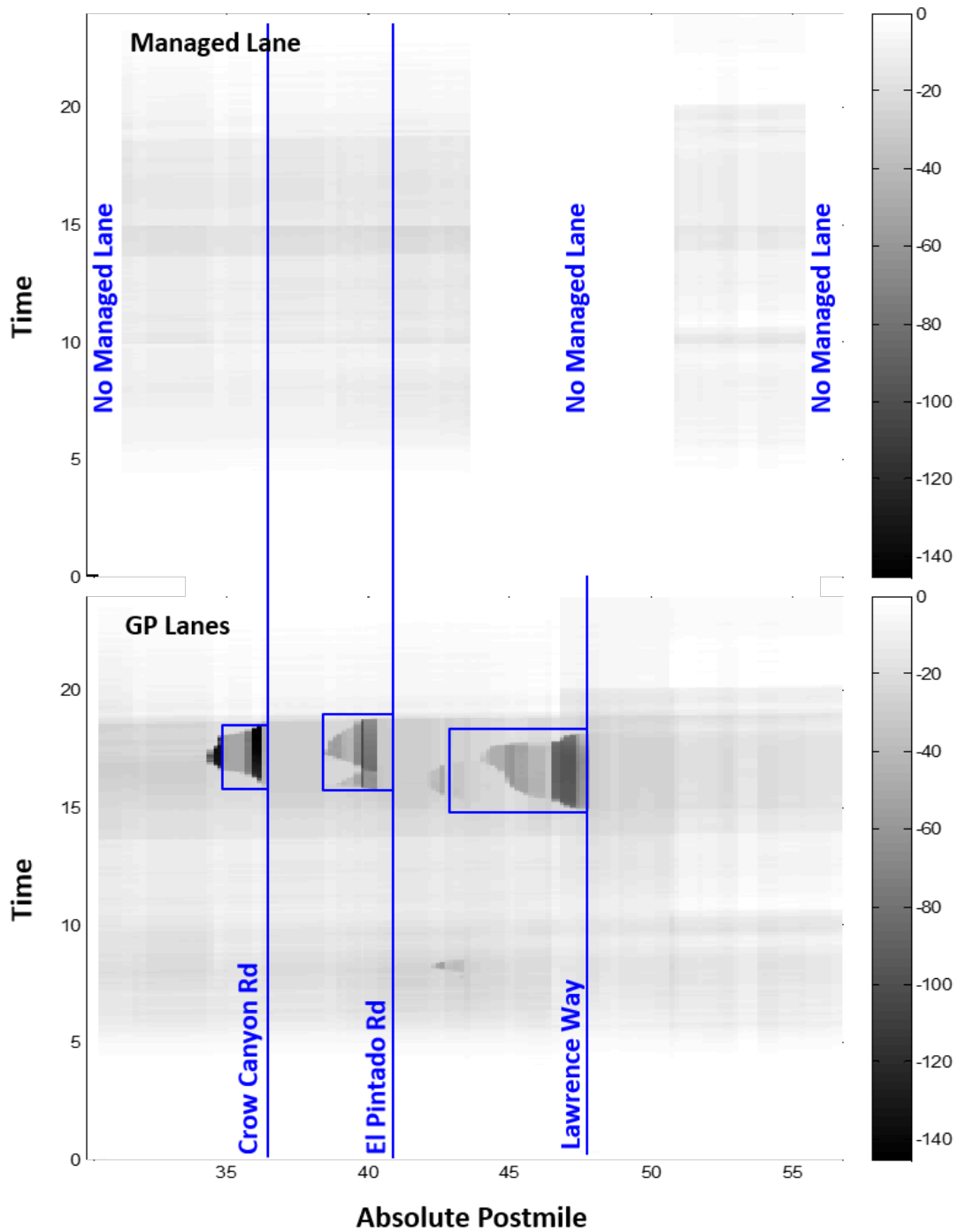


Figure 5: I-680 North density contours for GP and managed lanes produced by simulation. Density values are given in vehicles per mile per lane. Blue boxes on the GP lane speed contour indicate congested areas as identified by the I-680 CSMP study.

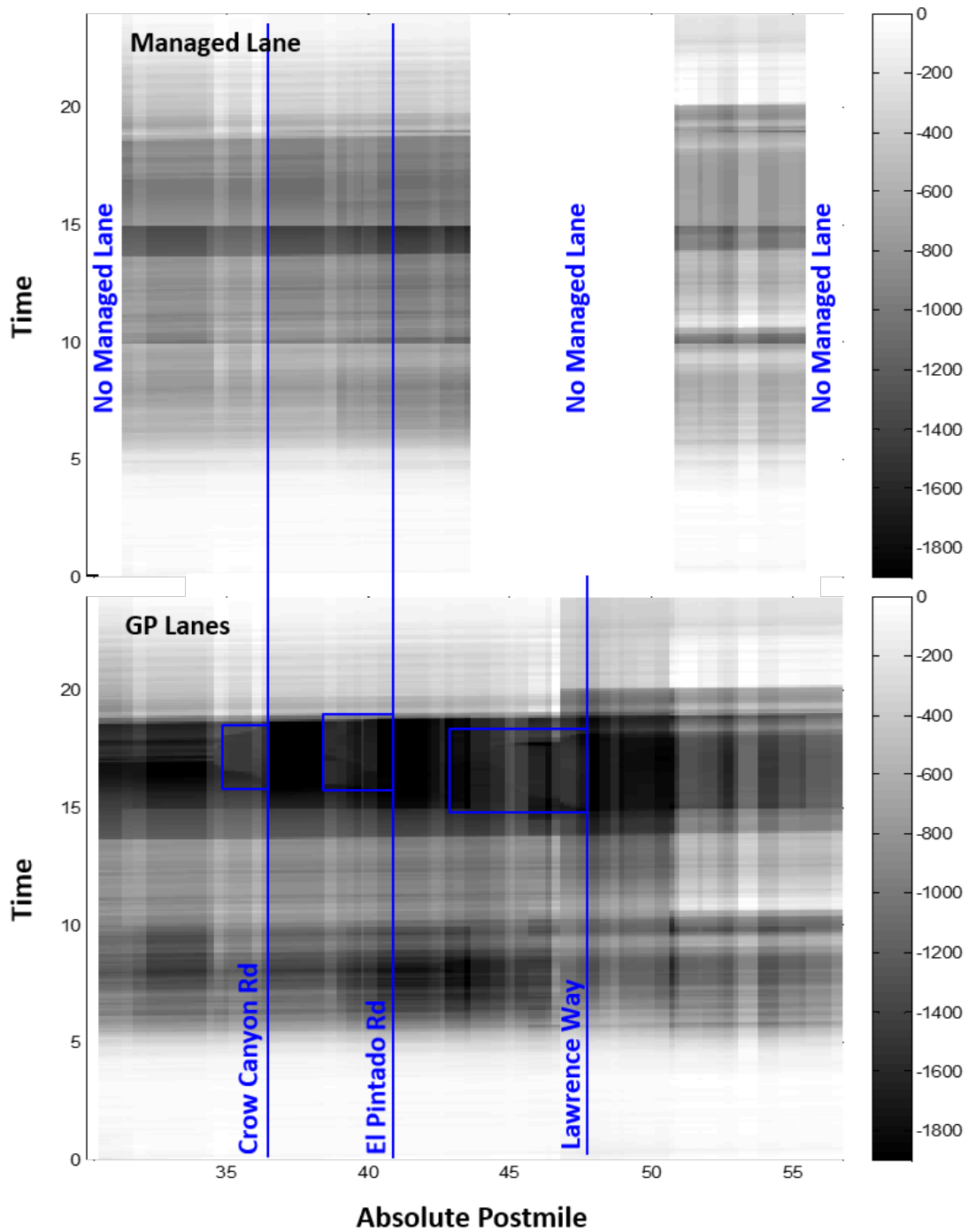


Figure 6: I-680 North flow contours for GP and managed lanes produced by simulation. Flow values are given in vehicles per hour per lane. Blue boxes on the GP lane speed contour indicate congested areas as identified by the I-680 CSMP study.

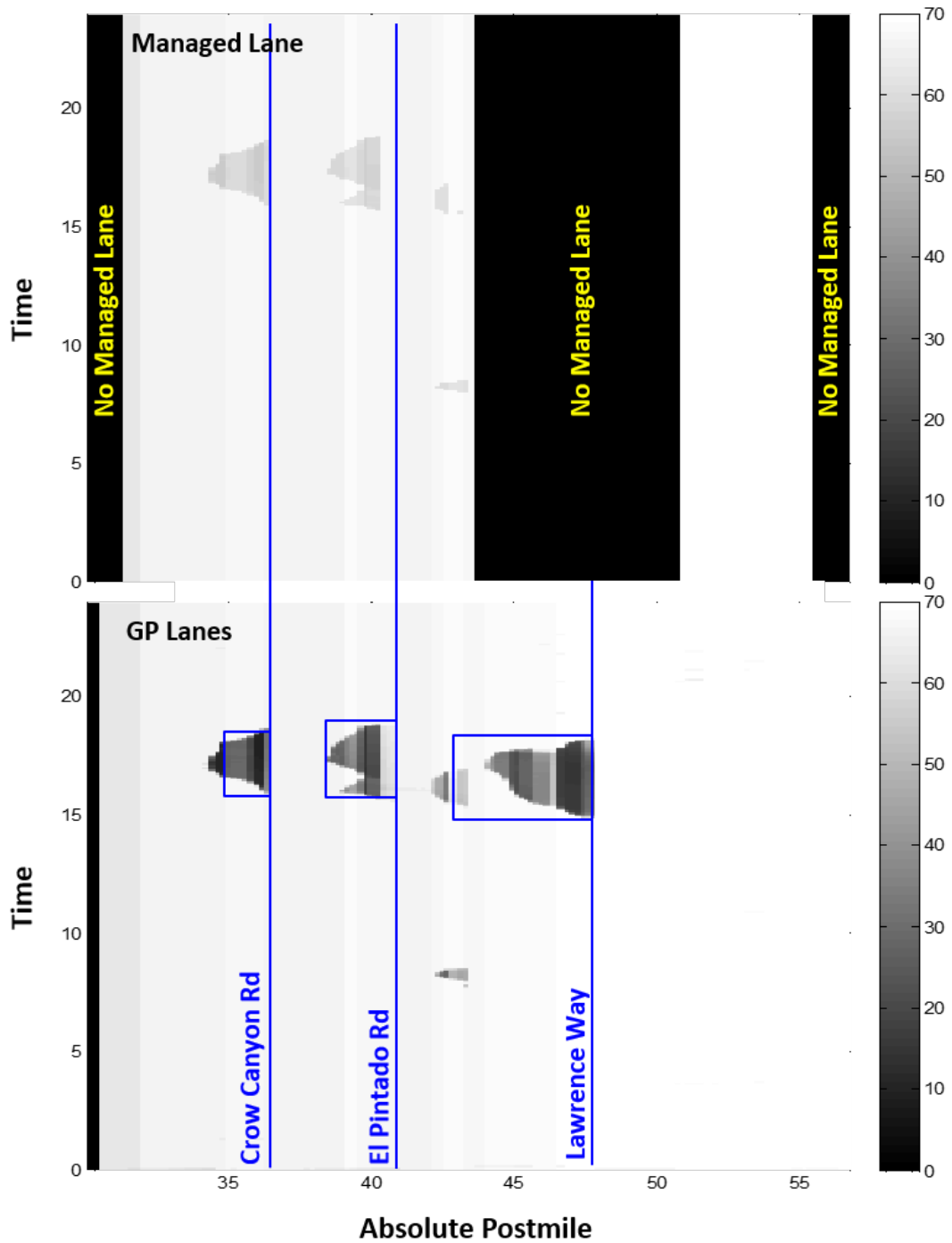


Figure 7: I-680 North speed contours for GP and managed lanes produced by simulation. Speed values are given in miles per hour. Blue boxes on the GP lane speed contour indicate congested areas as identified by the I-680 CSMP study.

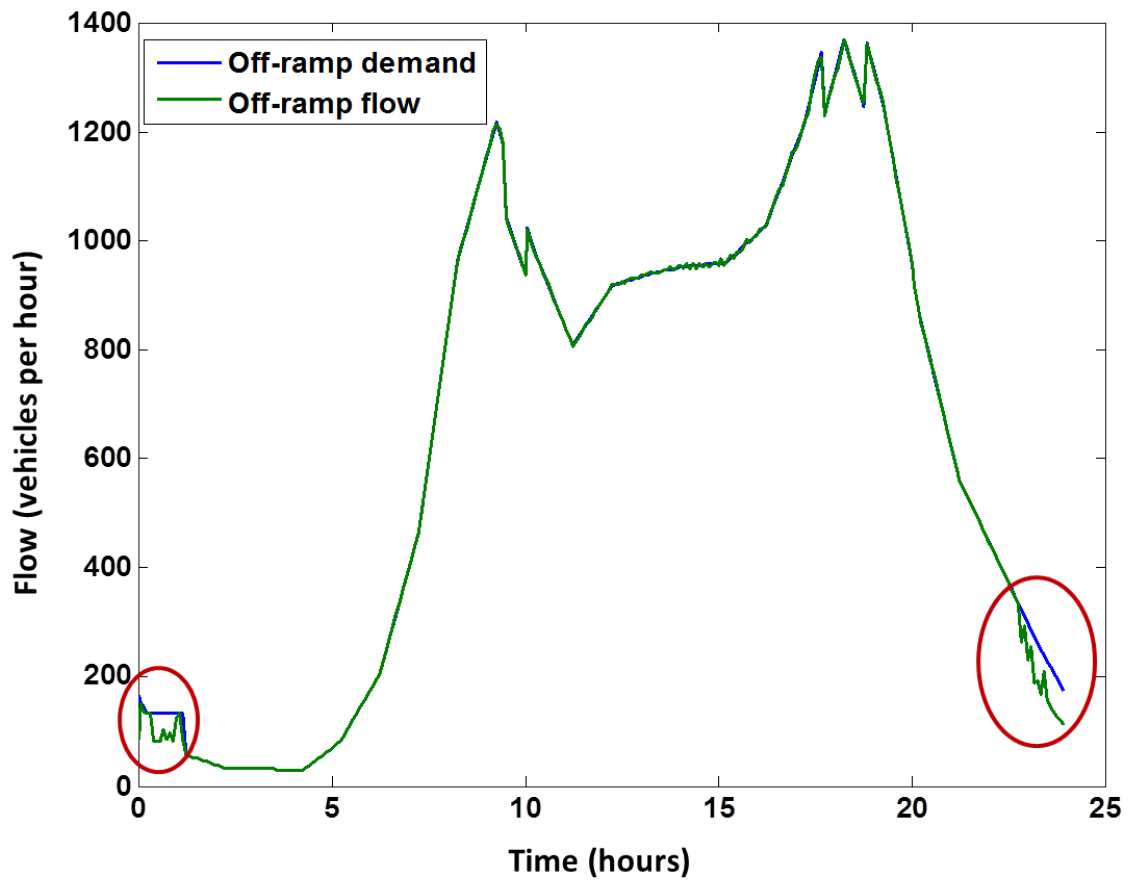


Figure 8: Flow at the Crow Canyon Road offramp over 24 hours — collected (offramp demand) vs. computed by simulation (offramp flow).



## 4.2 Gated-access managed lane case study: Interstate 210 East

We consider a 20.6-mile stretch of SR-134 East/ I-210 East in Los Angeles County, California, shown in Figure 9, as a test case for the separated managed lane configuration. This freeway’s managed lane is also an HOV lane. This freeway stretch consists of 3.9 miles of SR-134 East from postmile 9.46 to postmile 13.36, which merges into 16.7 miles of I-210 East from postmile 25 to postmile 41.7. Gate locations where traffic can switch between the GP and the HOV lanes are marked on the map. At this site, the HOV lane is always active. There are 28 onramps and 25 offramps. The largest number of offramps between two gates is 5. Thus, our freeway model has 7 vehicle classes - LOV (low-occupancy vehicles; not managed lane-eligible), HOV (managed lane-eligible) and 5 destination-based.

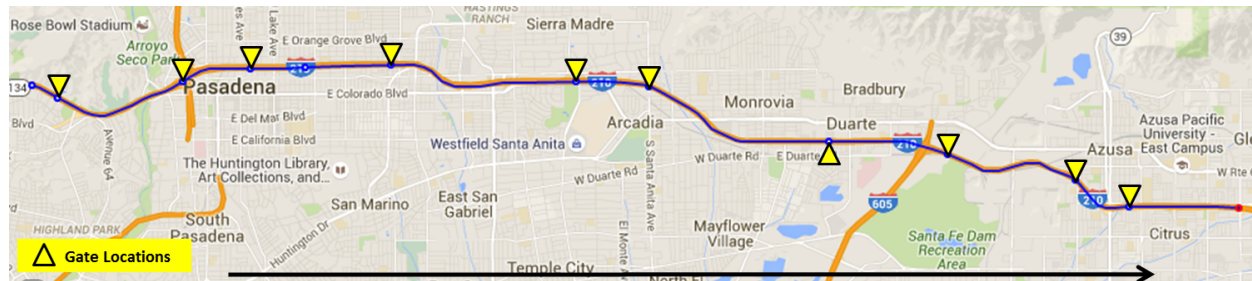


Figure 9: Map of SR-134 East/ I-210 East freeway in Los Angeles County.

To build the model, we used PeMS data for the corresponding segments of the SR-134 East and I-210 East for Monday, October 13, 2014 (PeMS, 2019). Fundamental diagrams were calibrated using PeMS data following the methodology of Dervisoglu et al. (2009). As in the I-680 North example, we assume that the managed lane-eligible portion of the input demand is 15%.

The modeling results are presented in Figures 10, 11 and 12 showing density, flow and speed contours, respectively, in the GP and the managed lanes. In each plot, the top contour corresponds to the managed lanes, and the bottom to the GP lanes. As before, in all the plots traffic moves from left to right along the “Absolute Postmile” axis, while the vertical axis represents time. The managed lane does not get congested. Dashed blue lines on the contour plots indicate managed gate locations.

Figure 13 shows the PeMS speed contours for the SR-134 East/ I-210 East GP and managed lanes that were used as a target for our simulation model. In these plots, traffic also travels from left to right, with the horizontal axis representing postmiles, while the vertical axis represents time.

Figure 14 shows an example of how well the offramp flow computed by the simulation matches the target, referred to as *offramp demand*, as recorded by the detector on the offramp at North Hill Avenue. The simulated offramp flow matches the offramp demand fairly closely. Similar results were found for the other offramps.

Finally, Table 2 summarizes the performance metrics — VMT, VHT and delay — computed by simulation versus those values obtained from PeMS. The PeMS data come from both SR-134 East and I-210 East, and VMT, VHT and delay values are computed as sums of the corresponding values from these two freeway sections. Delay values are computed in vehicle-hours for those vehicles traveling slower than 45 mph.

Performance metric	Simulation result	PeMS data
GP Lane VMT	2,017,322	-
Managed Lane VMT	378,485	-
Total VMT	2,395,807	$414,941 + 2,006,457 = 2,421,398$
GP Lane VHT	33,533	-
Managed Lane VHT	6,064	-
Total VHT	39,597	$6,416 + 36,773 = 43,189$
GP Lane Delay (hr)	3,078	-
Managed Lane Delay (hr)	584	-
Total Delay (hr)	3,662	$1 + 3,802 = 3,803$

Table 2: Performance metrics for SR-134 East/ I-210 East.

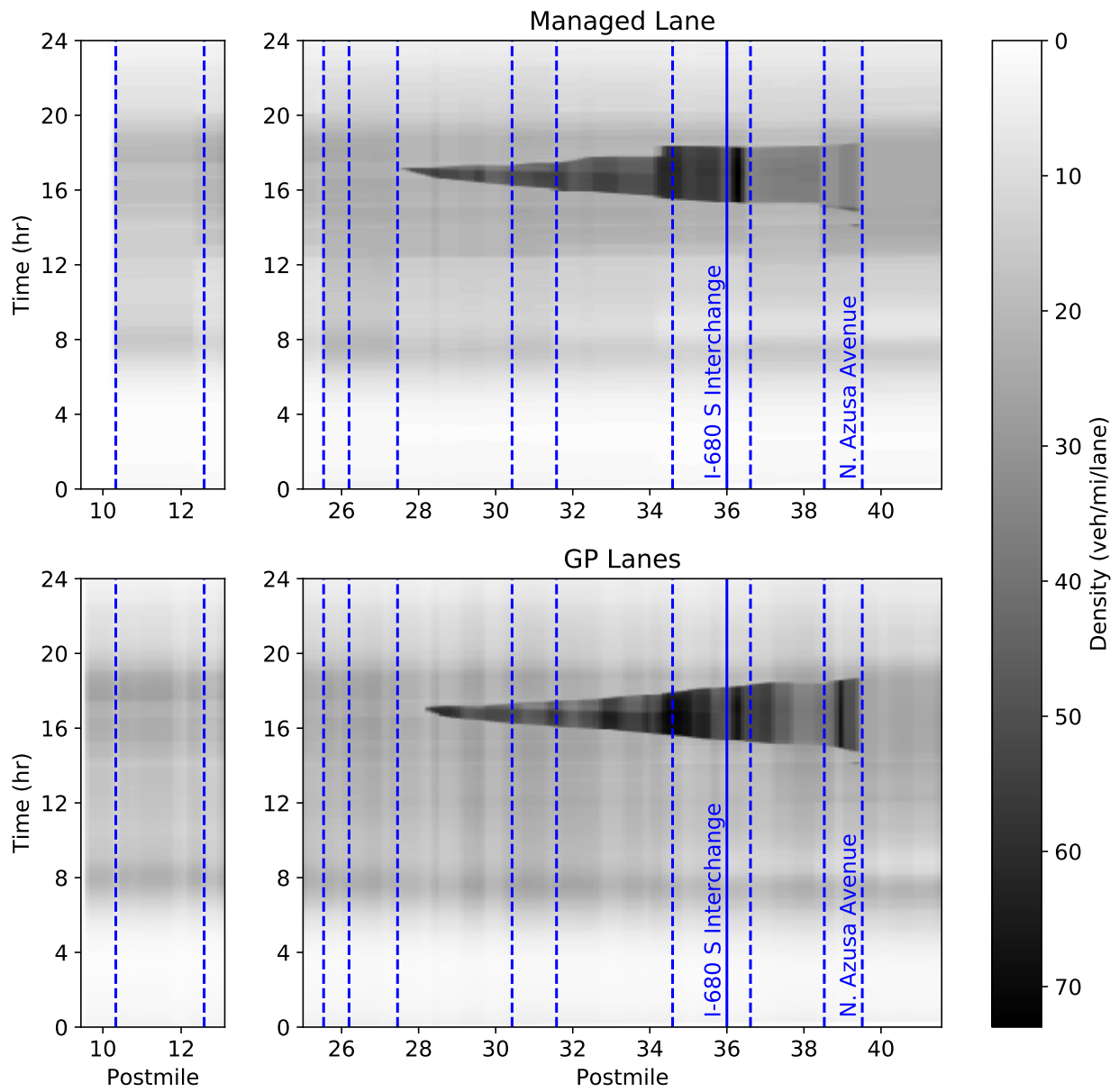


Figure 10: SR-134 East (left plots) / I-210 East (right plots) density contours for GP and managed lanes produced by simulation. Dotted blue lines represent the approximate position of the managed lane gates.

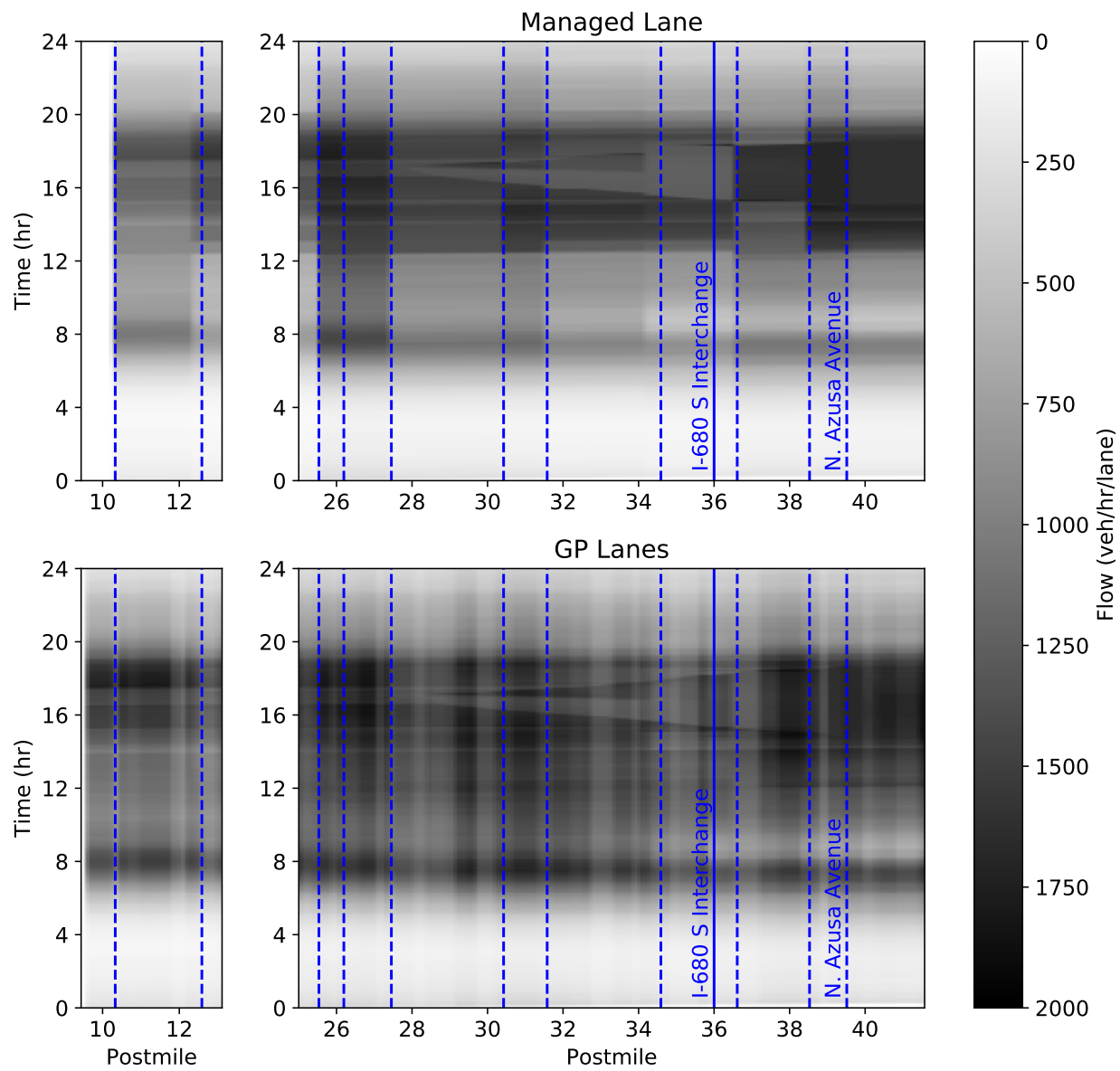


Figure 11: SR-134 East (left plots) / I-210 East (right plots) flow contours for GP and managed lanes produced by simulation. Dotted blue lines represent the approximate position of the managed lane gates.

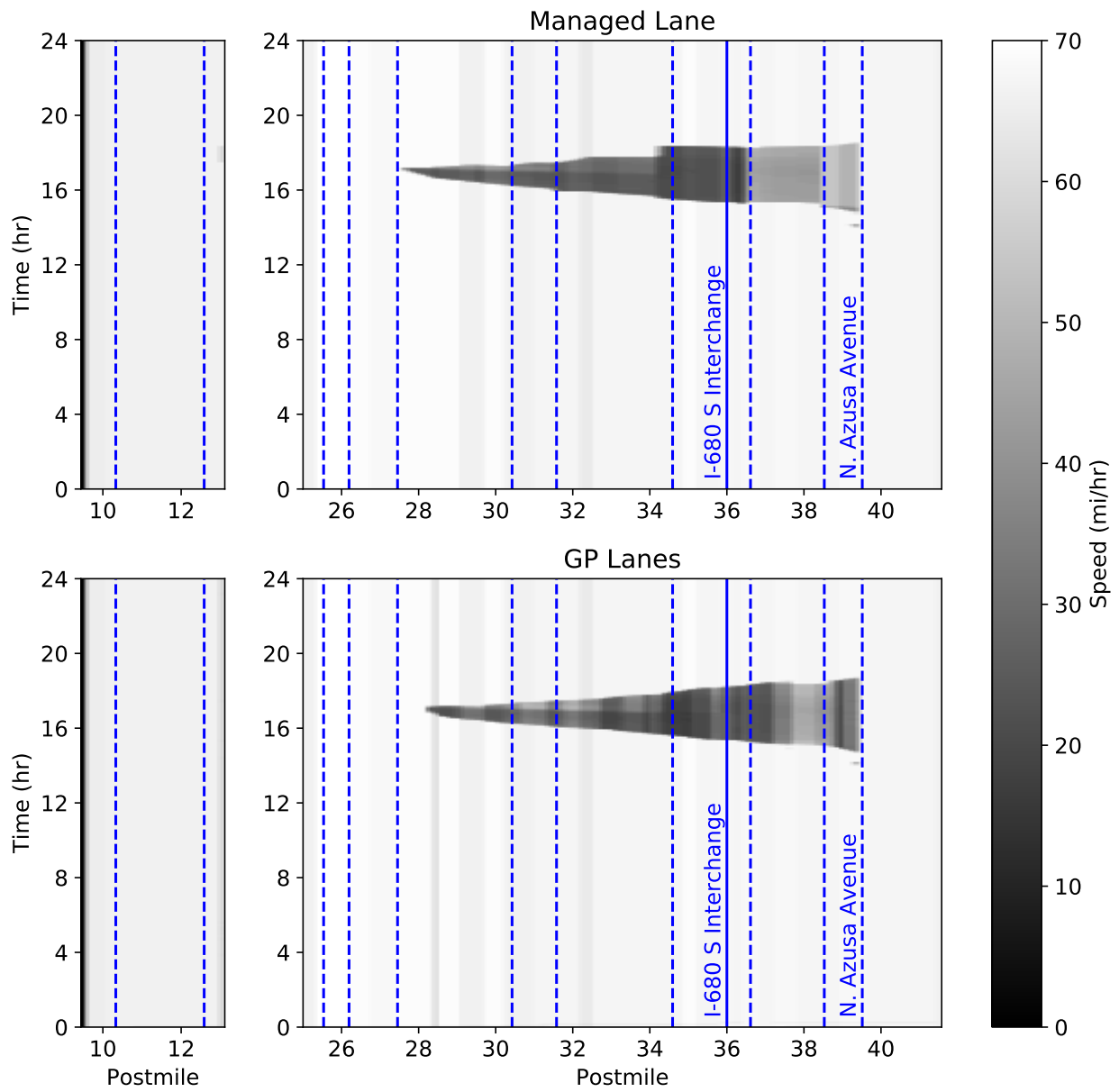


Figure 12: SR-134 East (left plots) / I-210 East (right plots) speed contours for GP and managed lanes produced by simulation. Dotted blue lines represent the approximate position of the managed lane gates.

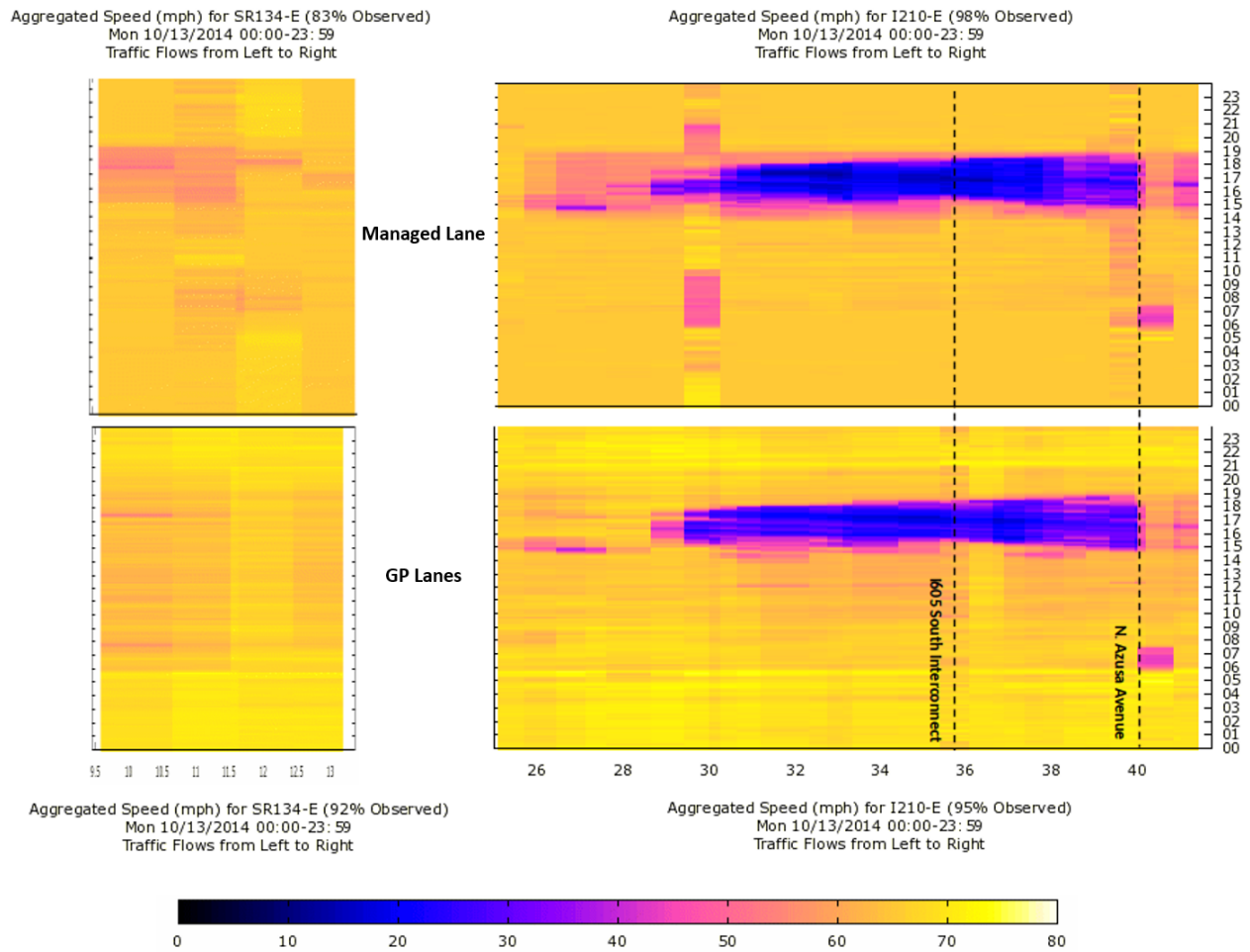


Figure 13: SR-134 East/ I-210 East speed contours for GP and managed lanes obtained from PeMS for Monday, October 13, 2014. The horizontal axis represents absolute postmile, and the vertical axis represents time in hours. Note the four contours share the same color scale.

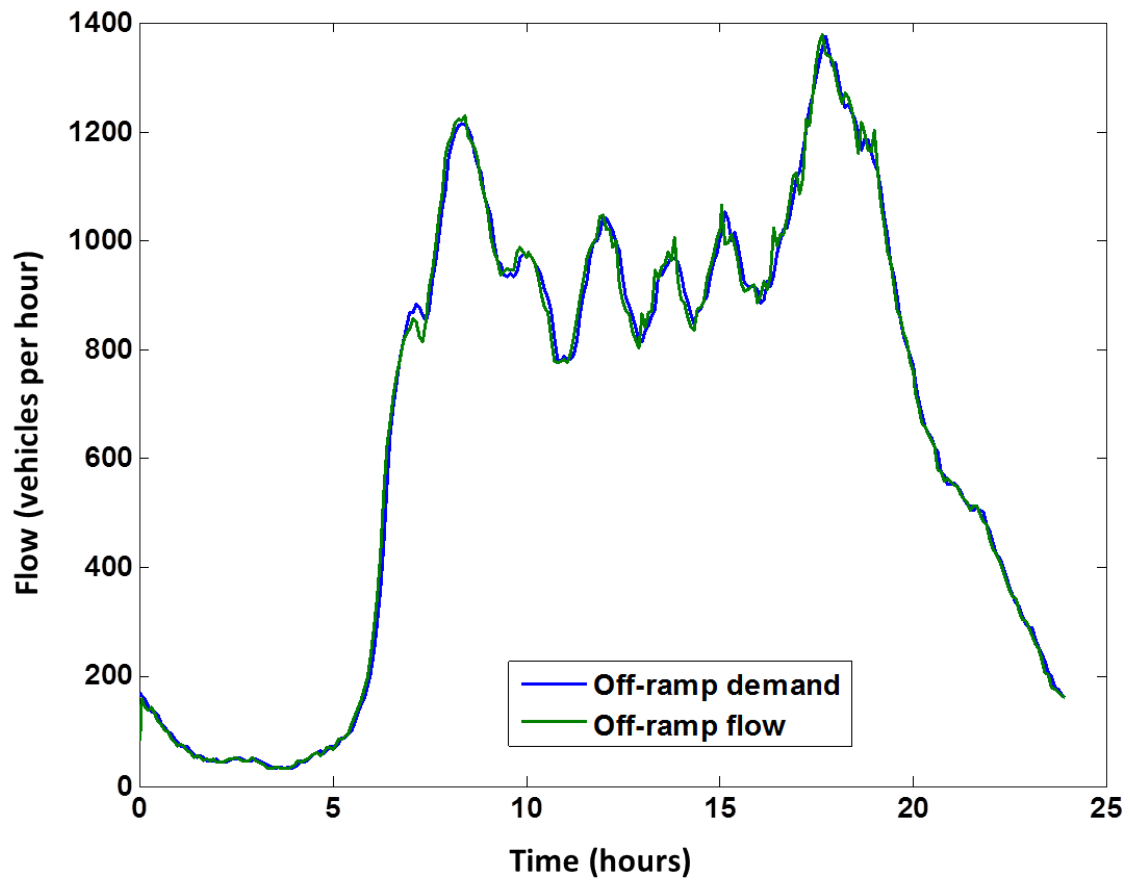


Figure 14: Flow at the North Hill Avenue offramp over 24 hours — PeMS data (offramp demand) vs. computed by simulation (offramp flow).

### 4.3 Discussion

As we mention in section 3, a common calibration goal for traffic modelers is to create a simulation that can accurately recreate a “base case” of a typical real-world day’s traffic patterns; this calibrated “base case” can then be tweaked to predict the system-wide effects of counterfactual events such as a global demand increase, a localized lane closure, etc.

One traditional criterion for evaluating whether a freeway model captures this “base case” is whether the simulation predicts congestion at the same time and the same place as in real-world data (and, if the dynamic behaviors such as the rate of the buildup of the queue and the rate of queue discharge are similar). In this congestion-locality criterion, our simulation case studies perform well. For the case study of I-680 North, examining Figures 5 through 7 we see that our models predict congestion originating at the bottleneck locations and propagating to the extents identified in the CSMP study (System Metrics Group, Inc., 2015). For the SR-134 East / I-210 East, we can compare the reference PeMS loop data speed contour (Figure 13) to our simulations (Figures 10-12). The PeMS data show and our simulations predict congestion in both the managed lane and the GP lanes that originates at a bottleneck at N. Azusa Avenue at roughly 15:00, propagates backward in space until reaching its maximum spatial extent roughly at postmile 29 at about 17:00, and then recedes until fully dissipating at roughly 19:00. The managed lane data from the PeMS dataset (Figure 13) has more identifiable wavefronts propagating backward and receding forward than the GP lanes, and those wavefront’s speeds agree somewhat with those predicted by the simulation (unfortunately, a definitive value for the true wavefront speed is difficult to obtain due to the low resolution of the PeMS data).

Beyond the somewhat qualitative examination of whether the macroscopic congestion matters match reality, we can also evaluate quantitatively whether our simulation fits the available measurements from the site. Figures 8 and 14 show how our model matched the offramp flow at the two identified bottlenecks of the case study sites. Both figures show agreement between model and data. Note that this “offramp demand” was an explicit calibration target (as described in section 3.3). So, close matching of this is an explicit requisite for the calibrated model, and, it is necessary that the offramp flow here be satisfied, and the flow that does not take the offramp still produce the congestion patterns as discussed in the previous paragraph. These two offramp flow figures can be interpreted as stating Neumann (flux) boundary conditions that our freeway PDE model must (and does) fulfill, in addition to the macro-scale congestion requirements.

Finally, Tables 1 and 2 show macroscopic freeway performance metrics predicted by our simulation and the comparable measured performance metrics. For the three quantities for which measured performance metrics are available (total VMT, total VHT, and total delay), we can see that all percentage errors between our simulation and the measurements are at most roughly 10%. We consider this is a fairly good accuracy, given the inherent high noise of performance metrics computed from stationary sensors like the loop detectors used by PeMS (Jia et al., 2001; Chen et al., 2003). In particular, we find higher errors between the simulated performance metrics and the measured performance metrics for the SR-134 East / I-210 East case study, a location where single-loop detectors are present, than for the I-680 North case study, where mostly dual-loop detectors are present (PeMS, 2019) (single-loop detectors being intrinsically much more noisy than dual-loop detectors at measuring quantities like speed and flow (Jia et al., 2001)).

## 5 Conclusion

This paper presented the implementation of the modeling components for managed lane-freeway networks originally proposed in Wright et al. (2019). This included their integration into both a full macroscopic traffic model suitable for corridor-scale traffic simulation and analysis, as well as fitting in estimation methods for some of the harder-to-estimate parameters into the traditional iterative calibration approach for traffic models.



Our simulation results comparing our model and calibration results showed good agreement in two case studies, validating both our full-access and gated-access modeling techniques. In the sequel to this paper series, we will further extend these results to include simulation and study of traffic control, with a reactive tolling controller on the managed lane.

## Acknowledgements

We would like to express great appreciation to several of our colleagues. To Elena Dorogush and Ajith Muralidharan for sharing ideas, and to Gabriel Gomes and Pravin Varaiya for their critical reading and their help in clarifying some theoretical issues.

This research was supported by the California Department of Transportation. Earlier versions of some of this article’s material previously appeared in the technical report Horowitz et al. (2016).

## A A link Model

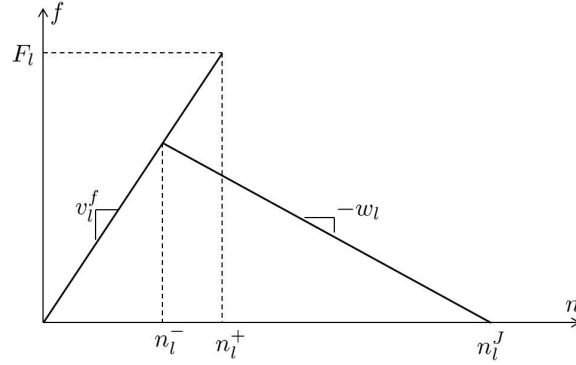


Figure 15: The “backwards lambda” fundamental diagram.

For the majority of this work, we remain agnostic as to the particular functional relationship between density  $\rho_l$ , demand  $S_l$  (per commodity,  $\rho_l^c$ ,  $S_l^c$ ) and supply  $R_l$ , and flow  $f_l$  (also called the fundamental diagram) used in our first-order macroscopic model. For the simulation results presented in section 4, we use a particular link model shown in Figure 15. This fundamental diagram captures the traffic hysteresis behavior with the “backwards lambda” shape often observed in detector data (Koshi et al., 1983):

$$S_l^c(t) = v_l^f(t) \rho_l^c(t) \min \left\{ 1, \frac{F_l(t)}{v_l^f(t) \sum_{c=1}^C \rho_l^c(t)} \right\}, \quad S_l(t) = \sum_{c=1}^C S_l^c(t), \quad (\text{A.1})$$

$$R_l(t) = (1 - \theta_l(t)) F_l(t) + \theta_l(t) w_l(t) \left( \rho_l^J(t) - \sum_{c=1}^C \rho_l^c(t) \right), \quad (\text{A.2})$$

where, for link  $l$ ,  $F_l$  is the capacity,  $v_l^f$  is the free flow speed,  $w_l$  is the congestion wave speed,  $\rho_l^J$  is the jam density, and  $\rho_l^- = \frac{w_l \rho_l^J}{v_l^f + w_l}$  and  $\rho_l^+ = \frac{F_l}{v_l^f}$  are called the *low* and *high critical densities*, respectively. As written here and used in this work,  $F_l$ ,  $v_l^f$ , and  $w_l$  are in units per simulation timestep. The variable  $\theta_l(t)$  is a congestion metastate of  $l$ , which encodes the hysteresis:

$$\theta_l(t) = \begin{cases} 0 & \rho_l(t) \leq \rho_l^-, \\ 1 & \rho_l(t) > \rho_l^+, \\ \theta_l(t-1) & \rho_l^- < \rho_l(t) \leq \rho_l^+, \end{cases} \quad (\text{A.3})$$

where  $\rho_l(t) = \sum_{c=1}^C \rho_l^c(t)$ .

Examining (A.3) and (A.2), we see that when a link's density goes above  $\rho_l^+$  (i.e., when it becomes congested), its ability to receive flow is reduced until the density falls below  $\rho_l^-$ .

An image of (A.1) and (A.2) overlaid on each other, giving a schematic image of the fundamental diagram, is shown in Figure 15. Unless  $\rho_l^- = \rho_l^+$ , when it assumes triangular shape, the fundamental diagram is not a function of density alone (i.e., without  $\theta_l(t)$ ):  $\rho_l(t) \in (\rho_l^-, \rho_l^+]$  admits two possible flow values.

## B Dynamic Split Ratio Solver

Throughout this article, we have made reference to a dynamic-system-based method for solving for partially- or fully-undefined split ratios from Wright et al. (2017). This split ratio solver is designed to implicitly solve the logit-based split ratio problem

$$\beta_{ij}^c = \frac{\exp\left(\frac{\sum_{i=1}^M \sum_{c=1}^C S_{ij}^c}{R_j}\right)}{\sum_{j'=1}^N \exp\left(\frac{\sum_{i=1}^M \sum_{c=1}^C S_{ij'}^c}{R_{j'}}\right)}, \quad (\text{B.1})$$

which cannot be solved explicitly, as the  $S_{ij}^c$ 's are also functions of the  $\beta_{ij}^c$ 's. The problem (B.1) is chosen to be a node-local problem that does not rely on information from the link model (beyond supplies and demands), and is thus independent of the choice of link model (Wright et al., 2017).

The solution algorithm is as follows, reproduced from Wright et al. (2017). More discussion is available in the reference.

- Define the set of commodity movements for which split ratios are known as  $\mathcal{B} = \{\{i, j, c\} : \beta_{ij}^c \in [0, 1]\}$ , and the set of commodity movements for which split ratios are to be computed as  $\overline{\mathcal{B}} = \{\{i, j, c\} : \beta_{ij}^c \text{ are unknown}\}$ .
- For a given input link  $i$  and commodity  $c$  such that  $S_i^c = 0$ , assume that all split ratios are known:  $\{i, j, c\} \in \mathcal{B}$ .<sup>1</sup>
- Define the set of output links for which there exist unknown split ratios as  $V = \{j : \exists \{i, j, c\} \in \overline{\mathcal{B}}\}$ .
- Assuming that for a given input link  $i$  and commodity  $c$ , the split ratios must sum up to 1, define the unassigned portion of flow by  $\overline{\beta}_i^c = 1 - \sum_{j:\{i,j,c\} \in \mathcal{B}} \beta_{ij}^c$ .
- For a given input link  $i$  and commodity  $c$  such that there exists at least one commodity movement  $\{i, j, c\} \in \overline{\mathcal{B}}$ , assume  $\overline{\beta}_i^c > 0$ , otherwise the undefined split ratios can be trivially set to 0.
- For every output link  $j \in V$ , define the set of input links that have an unassigned demand portion directed toward this output link by  $U_j = \{i : \exists \{i, j, c\} \in \overline{\mathcal{B}}\}$ .
- For a given input link  $i$  and commodity  $c$ , define the set of output links for which split ratios for which are to be computed as  $V_i^c = \{j : \exists i \in U_j\}$ , and assume that if nonempty, this set contains at least two elements, otherwise a single split ratio can be trivially set equal to  $\overline{\beta}_i^c$ .
- Assume that input link priorities are non-negative,  $p_i \geq 0$ ,  $i = 1, \dots, M$ , and  $\sum_{i=1}^M p_i = 1$ .

<sup>1</sup>If split ratios were undefined in this case, they could be assigned arbitrarily.

- Define the set of input links with zero priority:  $U_{zp} = \{i : p_i = 0\}$ . To enable split ratio assignment for inputs with zero priorities, perform regularization:

$$\tilde{p}_i = p_i \left(1 - \frac{|U_{zp}|}{M}\right) + \frac{1}{M} \frac{|U_{zp}|}{M} = p_i \frac{M - |U_{zp}|}{M} + \frac{|U_{zp}|}{M^2}, \quad (\text{B.2})$$

where  $|U_{zp}|$  denotes the number of elements in set  $U_{zp}$ . Expression (B.2) implies that the regularized input priority  $\tilde{p}_i$  consists of two parts: (1) the original input priority  $p_i$  normalized to the portion of input links with positive priorities; and (2) uniform distribution among  $M$  input links,  $\frac{1}{M}$ , normalized to the portion of input links with zero priorities.

Note that the regularized priorities  $\tilde{p}_i > 0$ ,  $i = 1, \dots, M$ , and  $\sum_{i=1}^M \tilde{p}_i = 1$ .

The algorithm for distributing  $\bar{\beta}_i^c$  among the commodity movements in  $\bar{\mathcal{B}}$  (that is, assigning values to the a priori unknown split ratios) aims at maintaining output links as uniform in their demand-supply ratios as possible. At each iteration  $k$ , two quantities are identified:  $\mu^+(k)$ , which is the largest *oriented* demand-supply ratio produced by the split ratios that have been assigned so far, and  $\mu^-(k)$ , which is the smallest oriented demand-supply ratio whose input link, denoted  $i^-$ , still has some unclaimed split ratio. Once these two quantities are found, the commodity  $c^-$  in  $i^-$  with the smallest unallocated demand has some of its demand directed to the  $j$  corresponding to  $\mu^-(k)$  to bring  $\mu^-(k)$  up to  $\mu^+(k)$  (or, if this is not possible due to insufficient demand, all such demand is directed).

To summarize, in each iteration  $k$ , the algorithm attempts to bring the smallest oriented demand-supply ratio  $\mu^+(k)$  up to the largest oriented demand-supply ratio  $\mu^-(k)$ . If it turns out that all such oriented demand-supply ratios become perfectly balanced, then the demand-supply ratios  $(\sum_i \sum_c S_{ij}^c)/R_j$  are as well.

The algorithm is:

1. Initialize:

$$\begin{aligned} \tilde{\beta}_{ij}^c(0) &:= \begin{cases} \beta_{ij}^c, & \text{if } \{i, j, c\} \in \mathcal{B}, \\ 0, & \text{otherwise;} \end{cases} \\ \bar{\beta}_i^c(0) &:= \bar{\beta}_i^c; \\ \tilde{U}_j(0) &= U_j; \\ \tilde{V}(0) &= V; \\ k &:= 0, \end{aligned}$$

Here  $\tilde{U}_j(k)$  is the remaining set of input links with some unassigned demand, which may be directed to output link  $j$ ; and  $\tilde{V}(k)$  is the remaining set of output links, to which the still-unassigned demand may be directed.

2. If  $\tilde{V}(k) = \emptyset$ , stop. The sought-for split ratios are  $\{\tilde{\beta}_{ij}^c(k)\}$ ,  $i = 1, \dots, M$ ,  $j = 1, \dots, N$ ,  $c = 1, \dots, C$ .

3. Calculate the remaining unallocated demand:

$$\bar{S}_i^c(k) = \bar{\beta}_i^c(k) S_i^c, \quad i = 1, \dots, M, \quad c = 1, \dots, C.$$

4. For all input-output link pairs, calculate oriented demand:

$$\tilde{S}_{ij}^c(k) = \tilde{\beta}_{ij}^c(k) S_i^c.$$

5. For all input-output link pairs, calculate oriented priorities:

$$\tilde{p}_{ij}(k) = \tilde{p}_i \frac{\sum_{c=1}^C \gamma_{ij}^c S_i^c}{\sum_{c=1}^C S_i^c} \quad (\text{B.3})$$

with

$$\gamma_{ij}^c(k) = \begin{cases} \beta_{ij}^c, & \text{if split ratio is defined a priori: } \{i, j, c\} \in \mathcal{B}, \\ \tilde{\beta}_{ij}^c(k) + \frac{\bar{\beta}_i^c(k)}{|V_i^c|}, & \text{otherwise,} \end{cases} \quad (\text{B.4})$$

where  $|V_i^c|$  denotes the number of elements in the set  $V_i^c$ . Examining the expression (B.3)-(B.4), one can see that the split ratios  $\tilde{\beta}_{ij}^c(k)$ , which are not fully defined yet, are complemented with a fraction of  $\bar{\beta}_i^c(k)$  inversely proportional to the number of output links among which the flow of commodity  $c$  from input link  $i$  can be distributed.

Note that in this step we are using *regularized* priorities  $\tilde{p}_i$  as opposed to the original  $p_i$ ,  $i = 1, \dots, M$ . This is done to ensure that inputs with  $p_i = 0$  are not ignored in the split ratio assignment.

6. Find the largest oriented demand-supply ratio:

$$\mu^+(k) = \max_j \max_i \frac{\sum_{c=1}^C \tilde{S}_{ij}^c(k)}{\tilde{p}_{ij}(k) R_j} \sum_{i \in U_j} \tilde{p}_{ij}(k).$$

7. Define the set of all output links in  $\tilde{V}(k)$ , where the minimum of the oriented demand-supply ratio is achieved:

$$Y(k) = \arg \min_{j \in \tilde{V}(k)} \min_{i \in U_j(k)} \frac{\sum_{c=1}^C \tilde{S}_{ij}^c(k)}{\tilde{p}_{ij}(k) R_j} \sum_{i \in U_j} \tilde{p}_{ij}(k),$$

and from this set pick the output link  $j^-$  with the smallest output demand-supply ratio (when there are multiple minimizing output links, any of the minimizing output links may be chosen as  $j^-$ ):

$$j^- = \arg \min_{j \in Y(k)} \frac{\sum_{i=1}^M \sum_{c=1}^C \tilde{S}_{ij}^c(k)}{R_j}.$$

8. Define the set of all input links, where the minimum of the oriented demand-supply ratio for the output link  $j^-$  is achieved:

$$W_{j^-}(k) = \arg \min_{i \in \tilde{U}_{j^-}(k)} \frac{\sum_{c=1}^C \tilde{S}_{ij^-}^c(k)}{\tilde{p}_{ij^-}(k) R_{j^-}} \sum_{i \in U_{j^-}} \tilde{p}_{ij^-}(k),$$

and from this set pick the input link  $i^-$  and commodity  $c^-$  with the smallest remaining unallocated demand:

$$\{i^-, c^-\} = \arg \min_{\substack{i \in W_{j^-}(k), \\ c : \bar{\beta}_{i^-}^c(k) > 0}} \bar{S}_i^c(k).$$

9. Define the smallest oriented demand-supply ratio:

$$\mu^-(k) = \frac{\sum_{c=1}^C \tilde{S}_{i^-j^-}^c(k)}{\tilde{p}_{i^-j^-}(k) R_{j^-}} \sum_{i \in U_{j^-}} \tilde{p}_{ij^-}(k).$$

- If  $\mu^-(k) = \mu^+(k)$ , the oriented demands created by the split ratios that have been assigned as of iteration  $k$ ,  $\tilde{\beta}_{ij}^c(k)$ , are perfectly balanced among the output links, and to maintain this, all remaining unassigned split ratios should be distributed proportionally to the allocated supply:

$$\begin{aligned}\tilde{\beta}_{ij}^c(k+1) &= \tilde{\beta}_{ij}^c(k) + \frac{R_j}{\sum_{j' \in V_i^c(k)} R_{j'}} \bar{\beta}_i^c(k), \quad c: \bar{\beta}_i^c(k) > 0, \quad i \in \tilde{U}_j(k), \quad j \in \tilde{V}(k); \quad (\text{B.5}) \\ \bar{\beta}_i^c(k+1) &= 0, \quad c: \bar{\beta}_i^c(k) > 0, \quad i \in \tilde{U}_j(k), \quad j \in \tilde{V}(k); \\ \tilde{U}_j(k+1) &= \emptyset, \quad j \in \tilde{V}(k); \\ \tilde{V}(k+1) &= \emptyset.\end{aligned}$$

If the algorithm ends up at this point, we have emptied  $\tilde{V}(k+1)$  and are done.

- Else, assign:

$$\Delta \tilde{\beta}_{i^-j^-}^{c^-}(k) = \min \left\{ \bar{\beta}_{i^-}^{c^-}(k), \left( \frac{\mu^+(k) \tilde{p}_{i^-j^-}(k) R_{j^-}}{\bar{S}_{i^-}^{c^-}(k) \sum_{i \in U_{j^-}} \tilde{p}_{ij^-}(k)} - \frac{\sum_{c=1}^C \tilde{S}_{i^-j^-}^c(k)}{\bar{S}_{i^-}^{c^-}(k)} \right) \right\}; \quad (\text{B.6})$$

$$\tilde{\beta}_{i^-j^-}^{c^-}(k+1) = \tilde{\beta}_{i^-j^-}^{c^-}(k) + \Delta \tilde{\beta}_{i^-j^-}^{c^-}(k); \quad (\text{B.7})$$

$$\bar{\beta}_{i^-}^{c^-}(k+1) = \bar{\beta}_{i^-}^{c^-}(k) - \Delta \tilde{\beta}_{i^-j^-}^{c^-}(k); \quad (\text{B.8})$$

$$\tilde{\beta}_{ij}^c(k+1) = \tilde{\beta}_{ij}^c(k) \text{ for } \{i, j, c\} \neq \{i^-, j^-, c^-\};$$

$$\bar{\beta}_i^c(k+1) = \bar{\beta}_i^c(k) \text{ for } \{i, c\} \neq \{i^-, c^-\};$$

$$\tilde{U}_j(k+1) = \tilde{U}_j(k) \setminus \left\{ i: \bar{\beta}_i^c(k+1) = 0, \quad c = 1, \dots, C \right\}, \quad j \in \tilde{V}(k);$$

$$\tilde{V}(k+1) = \tilde{V}(k) \setminus \left\{ j: \tilde{U}_j(k+1) = \emptyset \right\}.$$

In (B.6), we take the minimum of the remaining unassigned split ratio portion  $\bar{\beta}_{i^-}^{c^-}(k)$  and the split ratio portion needed to equalize  $\mu^-(k)$  and  $\mu^+(k)$ . To better understand the latter, the second term in  $\min\{\cdot, \cdot\}$  can be rewritten as:

$$\frac{\mu^+(k) \tilde{p}_{i^-j^-}(k) R_{j^-}}{\bar{S}_{i^-}^{c^-}(k) \sum_{i \in U_{j^-}} \tilde{p}_{ij^-}(k)} - \frac{\sum_{c=1}^C \tilde{S}_{i^-j^-}^c(k)}{\bar{S}_{i^-}^{c^-}(k)} = \left( \frac{\mu^+(k)}{\mu^-(k)} - 1 \right) \left( \sum_{c=1}^C \tilde{S}_{i^-j^-}^c(k) \right) \frac{1}{\bar{S}_{i^-}^{c^-}(k)}.$$

The right hand side of the last equality can be interpreted as: flow that must be assigned for input  $i^-$ , output  $j^-$  and commodity  $c^-$  to equalize  $\mu^-(k)$  and  $\mu^+(k)$  minus flow that is already assigned for  $\{i^-, j^-, c^-\}$ , divided by the remaining unassigned portion of demand of commodity  $c^-$  coming from input link  $i^-$ .

In (B.7) and (B.8), the assigned split ratio portion is incremented and the unassigned split ratio portion is decremented by the computed  $\Delta \tilde{\beta}_{i^-j^-}^{c^-}(k)$ .

10. Set  $k := k + 1$  and return to step 2.

## References

- Caltrans Office of Project Development Procedures. How Caltrans Builds Projects, Aug. 2011. URL [http://www.dot.ca.gov/hq/tpp/index\\_files/How\\_Caltrans\\_Builds\\_Projects\\_HCBP\\_2011a-9-13-11.pdf](http://www.dot.ca.gov/hq/tpp/index_files/How_Caltrans_Builds_Projects_HCBP_2011a-9-13-11.pdf).
- M. J. Cassidy, K. Jang, and C. F. Daganzo. The smoothing effect of carpool lanes on freeway bottlenecks. *Transportation Research Part A: Policy and Practice*, 44(2):65–75, Feb. 2010. ISSN 09658564. doi: 10.1016/j.tra.2009.11.002.
- M. Chang, J. Wiegmann, A. Smith, and C. Bilotto. A Review of HOV Lane Performance and Policy Options in the United States. Report FHWA-HOP-09-029, Federal Highway Administration, 2008.

- C. Chen, J. Kwon, J. Rice, A. Skabardonis, and P. Varaiya. Detecting Errors and Imputing Missing Data for Single-Loop Surveillance Systems. *Transportation Research Record*, 1855(1):160–167, Jan. 2003. ISSN 0361-1981. doi: 10.3141/1855-20.
- C. F. Daganzo. The cell transmission model: A dynamic representation of highway traffic consistent with the hydrodynamic theory. *Transportation Research Part B: Methodological*, 28(4):269–287, Aug. 1994. doi: 10.1016/0191-2615(94)90002-7.
- C. F. Daganzo. The cell transmission model, Part II: Network traffic. *Transportation Research Part B: Methodological*, 29(2):79–93, Apr. 1995. ISSN 01912615. doi: 10.1016/0191-2615(94)00022-R.
- G. Dervisoglu, G. Gomes, J. Kwon, A. Muralidharan, P. Varaiya, and R. Horowitz. Automatic calibration of the fundamental diagram and empirical observations on capacity. *88th Annual Meeting of the Transportation Research Board, Washington, D.C., USA*, 2009.
- N. Farhi, H. Haj-Salem, M. Khoshyaran, J.-P. Lebacque, F. Salvarani, B. Schnetzler, and F. De Vuyst. The Logit lane assignment model: First results. In *Transportation Research Board 92nd Annual Meeting Compendium of Papers*, 2013.
- K. Fitzpatrick, R. Avelar, and T. E. Lindheimer. Operating Speed on a Buffer-Separated Managed Lane. *Transportation Research Record: Journal of the Transportation Research Board*, 2616(1):1–9, Jan. 2017. ISSN 0361-1981, 2169-4052. doi: 10.3141/2616-01.
- M. Fransson and M. Sandin. *Framework for Calibration of a Traffic State Space Model*. Masters Thesis, Linköping University, Norrköping, Sweden, Oct. 2012.
- R. Horowitz, A. A. Kurzhanskiy, A. Siddiqui, and M. A. Wright. Modeling and Control of HOT Lanes. Technical report, Partners for Advanced Transportation Technologies, University of California, Berkeley, Berkeley, CA, 2016. URL <https://escholarship.org/uc/item/9mx3903c>.
- K. Jang and M. J. Cassidy. Dual influences on vehicle speed in special-use lanes and critique of US regulation. *Transportation Research Part A: Policy and Practice*, 46(7):1108–1123, Aug. 2012. ISSN 09658564. doi: 10.1016/j.tra.2012.01.008.
- K. Jang, S. Oum, and C.-Y. Chan. Traffic Characteristics of High-Occupancy Vehicle Facilities: Comparison of Contiguous and Buffer-Separated Lanes. *Transportation Research Record: Journal of the Transportation Research Board*, 2278:180–193, Dec. 2012. ISSN 0361-1981. doi: 10.3141/2278-20.
- Z. Jia, C. Chen, B. Coifman, and P. Varaiya. The PeMS algorithms for accurate, real-time estimates of g-factors and speeds from single-loop detectors. In *2001 IEEE Intelligent Transportation Systems Proceedings*, pages 536–541. IEEE, 2001. ISBN 0-7803-7194-1. doi: 10.1109/ITSC.2001.948715.
- M. Koshi, M. Iwasaki, and I. Ohkura. Some findings and an overview on vehicular flow characteristics. In *Proceedings of the 8th International Symposium on Transportation and Traffic Flow Theory*, volume 198, pages 403–426, 1983.
- A. A. Kurzhanskiy and P. Varaiya. Traffic management: An outlook. *Economics of Transportation*, 4(3): 135–146, Sept. 2015. ISSN 22120122. doi: 10.1016/j.ecotra.2015.03.002.
- M. J. Lighthill and G. B. Whitham. On kinematic waves I. Flood movement in long rivers. *Proceedings of the Royal Society of London. Series A. Mathematical and Physical Sciences*, 229(1178):281–316, May 1955a. doi: 10.1098/rspa.1955.0088.
- M. J. Lighthill and G. B. Whitham. On kinematic waves II. A theory of traffic flow on long crowded roads. *Proceedings of the Royal Society of London. Series A. Mathematical and Physical Sciences*, 229(1178): 317–345, May 1955b. ISSN 2053-9169. doi: 10.1098/rspa.1955.0089.
- X. Liu, B. Schroeder, T. Thomson, Y. Wang, N. Roupail, and Y. Yin. Analysis of Operational Interactions Between Freeway Managed Lanes and Parallel, General Purpose Lanes. *Transportation Research Record: Journal of the Transportation Research Board*, 2262:62–73, Dec. 2011. ISSN 0361-1981. doi: 10.3141/2262-07.

- Y. Lou, Y. Yin, and J. A. Laval. Optimal dynamic pricing strategies for high-occupancy/toll lanes. *Transportation Research Part C: Emerging Technologies*, 19(1):64–74, Feb. 2011. ISSN 0968090X. doi: 10.1016/j.trc.2010.03.008.
- M. Menendez and C. F. Daganzo. Effects of HOV lanes on freeway bottlenecks. *Transportation Research Part B: Methodological*, 41(8):809–822, Oct. 2007. ISSN 01912615. doi: 10.1016/j.trb.2007.03.001.
- Metropolitan Transportation Commission. Bay Area Express Lanes, 2019. URL <http://bayareaexpresslanes.org>.
- D. Ngoduy and M. Maher. Calibration of second order traffic models using continuous cross entropy method. *Transportation Research Part C: Emerging Technologies*, 24:102–121, Oct. 2012. ISSN 0968090X. doi: 10.1016/j.trc.2012.02.007.
- J. Obenberger. Managed Lanes: Combining Access Control, Vehicle Eligibility, and Pricing Strategies Can Help Mitigate Congestion and Improve Mobility on the Nation’s Busiest Roadways. *Public Roads*, 68(3):48–55, Nov/Dec 2004. URL <http://www.fhwa.dot.gov/publications/publicroads/04nov/08.cfm>. Publication Number FHWA-HRT-05-002.
- PeMS. California Performance Measurement System, 2019. URL <http://pems.dot.ca.gov>.
- A. Poole and A. Kotsialos. METANET Model Validation using a Genetic Algorithm. *IFAC Proceedings Volumes*, 45(24):7–12, Sept. 2012. ISSN 14746670. doi: 10.3182/20120912-3-BG-2031.00002.
- A. Poole and A. Kotsialos. Second order macroscopic traffic flow model validation using automatic differentiation with resilient backpropagation and particle swarm optimisation algorithms. *Transportation Research Part C: Emerging Technologies*, 71:356–381, Oct. 2016. ISSN 0968090X. doi: 10.1016/j.trc.2016.07.008.
- P. F. Richards. Shock waves on the highway. *Operations Research*, 4(1):42–51, 1956. doi: 10.1287/opre.4.1.42.
- System Metrics Group, Inc. Contra Costa County I-680 Corridor System Management Plan Final Report. Technical report, Caltrans District 4, 2015. URL [http://dot.ca.gov/hq/tpp/corridor-mobility/CSMPs/d4\\_CSMPs/D04\\_I680\\_CSMP\\_Final\\_Revised\\_Report\\_2015-05-29.pdf](http://dot.ca.gov/hq/tpp/corridor-mobility/CSMPs/d4_CSMPs/D04_I680_CSMP_Final_Revised_Report_2015-05-29.pdf).
- M. Treiber and A. Kesting. *Traffic Flow Dynamics*. Springer Berlin Heidelberg, Berlin, Heidelberg, 2013. ISBN 978-3-642-32459-8 978-3-642-32460-4. doi: 10.1007/978-3-642-32460-4.
- M. A. Wright, G. Gomes, R. Horowitz, and A. A. Kurzhanskiy. On node models for high-dimensional road networks. *Transportation Research Part B: Methodological*, 105:212–234, Nov. 2017. ISSN 01912615. doi: 10.1016/j.trb.2017.09.001.
- M. A. Wright, R. Horowitz, and A. A. Kurzhanskiy. A Dynamic-System-Based Approach to Modeling Driver Movements Across General-Purpose/Managed Lane Interfaces. In *Proceedings of the ASME 2018 Dynamic Systems and Controls Conference (DSCC)*, page V002T15A003. ASME, Sept. 2018. ISBN 978-0-7918-5190-6. doi: 10.1115/DSCC2018-9125.
- M. A. Wright, R. Horowitz, and A. A. Kurzhanskiy. Macroscopic Modeling, Calibration, and Simulation of Managed Lane-Freeway Networks, Part I: Topological and Phenomenological Modeling. *to be submitted to Transportation Research Part B: Methodological*, 2019. URL <https://arxiv.org/abs/1609.09470>.